DOI:
10.1109/TRO.2011.2127210

Document Version
Peer reviewed version

Rolling Indentation Probe for Tissue Abnormality Identification during Minimally Invasive Surgery

Hongbin Liu, Jichun Li, Xiaojing Song, Lakmal D. Seneviratne and Kaspar Althoefer

Abstract—**This paper presents a novel optical fiber based rolling indentation probe designed to measure the stiffness distribution of a soft tissue while rolling over the tissue surface during minimally invasive surgery. By fusing the measurements along rolling paths, the probe can generalize a mechanical image to visualize the stiffness distribution within the internal tissue structure. Since tissue abnormalities are often firmer than the surrounding organ or parenchyma, a surgeon then can localize abnormalities by analyzing the image.**

The performance of the developed probe was validated using simulated soft tissues. Results show that the probe can measure the both force and indentation depth accurately with different orientations when the probe approached to and rolled on the tissue surface. In addition, experiments for tumor identification through rolling indentation were conducted. The size and embedded depth of the tumor as well as the stiffness ratio between the tumor and tissue were varied during tests. Results demonstrate that the probe can effectively and accurately identify the embedded tumors.

I. Introduction

There have been notable advances in robotic-assisted minimally invasive surgery (MIS) or laparoscopic surgery in recent years [1], [2]. Distinct advantages of these robotic systems include high distal dexterity, enhanced 3D vision, motion scaling and tremor filtering as well as direct hand-eye coordination eliminating reversed tool motions. These advances result in improved ergonomics and also allow complex surgical procedures, which are usually difficult to be conducted by conventional minimally invasive means such as coronary artery bypass grafting [3] and mitral valve repair[4] to be effectively performed. However, the lack of force perception in current robot-aided MIS systems is still one of the major downsides of such systems.

The force perception, which is readily available during open surgery and usually partially available during traditional laparoscopic procedures provides the surgeon with valuable information regarding the nature of the investigated soft tissues and potential extent of the margins of the disease. The loss of such sensation during an operation can lead to a misjudgment and result in inadvertent injury to neighbouring organs or an incomplete surgical resection.

Manuscript received March 07, 2011.

H. Liu, J. Li, X. Song, L. D. Seneviratne and K. Althoefer are with the Centre for Robotic Research, Kings College London, UK (phone: +44 20 7848 2041; e-mail: hongbin.liu@kcl.ac.uk). L. D. Seneviratne is also with College of Engineering, Khalifa University of Science Technology & Research, Abu Dhabi, UAE.

The research leading to these results has been partially supported by the HANDLE project, which has received funding from the European Communitity's Seventh Framework Programme (FP7/2007-2013) under grant agreement ICT 231640

Recent studies have revealed that the lack of force perception during robotics-assisted surgery can lead to an increase in tissue trauma and accidental tissue damage [5]. Furthermore, without the force perception, there is a clear risk of leaving cancer behind after the resection and potentially resulting in positive surgical margins. During open procedures surgeons often avoid this by identifying the tumor and its boundaries by palpation and hence ensure that a negative margin is achieved and the cancer has been completely excised. In laparoscopic surgery, the restricted access to the surgical field precludes manual palpation and surgeons rely on other techniques in order to locate tumors.

The most common method is to use the laparoscopic instruments to probe the surface of an organ, using visual and limited force perception transmitted via the laparoscopic tools to locate the tumor. This technique is reported to be time consuming and ineffective especially with small tumors buried deeply under the tissue surface [6].

It is possible to use imaging modalities such as magnetic resonance imaging (MRI) or computed tomography (CT) imaging to identify such tumor locations pre-operatively. However, due to the deformability of soft tissue and movement introduced by the surgical procedure, it is very difficult to accurately register the pre-operative images to the intra-operative tumor locations [7]. To intra-operatively identify tumors, an MIS ultrasound probe can be used. However due to its low image resolution, it can be problematic to find small tumors or accurately determine their position [8]. Optical Coherence Tomography (OCT) is an imaging technique which can instantly visualize sub-surface abnormalities with micro-meter resolution. However the penetration depth of OCT is limited to 1 – 2 mm below tissue surface [9]. Hence OCT is incapable of locating deeply buried tumors. The elastography is a technique for generating images of tissue elasticity by propagating mechanical waves through the tissues [10-12]. This method is effective for detecting tumors as tumors are often stiffer than the normal tissues [13, 14]. The limitation is that elasticity images are difficulty to generate in real time [10].

Applying Instruments equipped with tactile sensors to palpate the soft tissue is another approach for identifying the tissue abnormalities during surgery. Sabatini et al. developed a finger-like system equipped with a tactile sensor which is made of fingertip piezoelectric polymer film. The system is capable of detecting differences in tissue mechanical properties via palpation [15]. Dargahi et al. developed a tactile sensor which can predict the stiffness of the touched object irrespective of the geometry and thickness of the object [16]. Xu et al. developed a snake-like robot which allows for intrinsic tactile sensing in environments with the space and

sterilization constraints of MIS [17]. In [18, 19], surgical graspers instrumented with tactile sensing capabilities were developed to detect the compliance of the grasped tissue. In [8], the feasibility of utilizing a tactile probe to localize lung tumors based on variations in tissue stiffness is discussed.

The results show that applying tactile sensors is promising for identifying tissue abnormalities during MIS. However, the aforementioned techniques are often conducted in a discrete manner e.g. localized palpations or tissue grasping. This can cause difficulties when attempting to identify tissue abnormalities through a large tissue area, since it is time consuming and careful calibration must be carried out to account for changing boundary conditions. In order to allow a surgeon to rapidly investigate the tissue, tactile sensor arrays can be used to "mechanically image" the stiffness distribution of soft tissue. By successively palpating the tissue using the tactile arrays, the distributed tactile image measured from multiple palpations can be combined into a panoramic view of the investigating tissue to visualize locations of the embedded tumors. The use of a transrectal probe equipped with tactile sensor arrays to identify prostate tumors has been reported in [20]. Devices instrumented with tactile sensor arrays have also been used to classify breast lesions [21-23], locate pulmonary tumors [6] and identify arteries during robotic surgery [24]. Results from such research demonstrate that tactile imaging performs well as diagnostic tools. However, to cover a large tissue area and investigate relative variations over that area, such sensing arrays must either be very large or again perform multiple discrete palpations.

As such, authors have developed a new rolling indentation approach for tissue abnormalities localization during MIS [25-28]. This approach employs a force-sensitive wheel to roll over a soft tissue organ, allowing the continuous and rapid measurement of the tissue stiffness as rolling takes place, thus obtaining the stiffness distribution of a large tissue area in short time. The abnormalities within soft tissue can be then readily identified through examination of the stiffness distribution. The major limitation of the above approach is that the rolling indentation depth needs to be kept constant throughout the experiment. In previous work this was achieved by preregistering the tissue surface before experiments [25, 26]. Preregistering a tissue surface is time consuming and if applied into MIS, the tissue shift during a surgery may induce inaccuracies to the surface registration.

The aim of this paper is to introduce a novel fiber-optic based rolling indentation probe which can measure the indentation depth of a roller and the tissue reaction force concurrently during rolling indentation. The integration of indentation depth with the tissue reaction force is an important step forward from the earlier work, since it is now possible to compute the distribution of stiffness for a large organ without prior tissue surface registration.

In addition, utilizing fiber-optic based sensing methods allows the proposed probe being easily miniaturized to fit through a standard trocar port of 11mm in diameter; and the use of non-electronics components in the probe allows it to endure standard clinical sterilization procedures.

Initial research leading to the work described in the paper was presented in [44]. Based on this earlier work we have advanced a number of points. First, the design of the rolling indentation probe has been improved to instrument a rolling element on the probe tip. Second, advanced methods for estimating the tissue stiffness have been implemented and the indentation depth measurement accuracy for different approaching angle of the probe has been validated. Moreover, experiments have been carried out to investigate the following aspects: 1) the effect of tissue stiffness on the accuracy of indentation depth measurements; 2) the effect of tumor size and depth to tumor identification using the developed probe; 3) the effect of the tumor-tissue stiffness ratio to tumor identification.

II. The Development of Rolling indentation probe

A. Literature Survey for Indentation Depth sensing

The indentation depth of a roller is given by the relative displacement of the tip of roller with respect to the soft tissue surface. Hence the indentation depth can be measured by acquiring the local tissue deformation when the roller rolls over the soft tissue. So far, a number of techniques have been developed to acquire the tissue deformation during MIS.

Intra-operative CT technique can provide information regarding soft tissue morphology and structure. It is particularly suitable for differentiating the bones from other tissues and thus has been often used in the image-guided surgeries [29-32] However, due to the cost and the radiation exposure associated with such techniques, they are not ideal for intra-operatively measuring the tissue deformation. The stereo vision technique is relatively inexpensive and practical for measuring the tissue deformation in real time. This technique utilizes two or more cameras to interpolate the three-dimensional (3D) information of a subject including the shape, texture and depth [33]. This technique has been used to recover the 3D structure of the operating field [34] and track the temporal motion of deformable tissue surfaces [35] during a MIS. While the applications of stereo vision in MIS are promising and progressing, one major downside is by the difficult in extracting features on curved and specular surfaces. During surgical procedures where internal organs with curved surfaces are surrounded in fluids, the stereo vision technique is not always effective [36]. To extract features on curved surfaces, the laser line scanner can be used. While such system provides high resolution 3D images, it is usually not in real-time and difficult to require feature information from moving objects. A more practical way to obtain the 3D information of a curved object in real time is the structured light technique [36, 37]. This technique utilizes a projector to project a known light pattern onto an object. The light pattern on the object is then viewed from a camera mounted next to the projector. Given the known position and orientation of both camera and projector, the shape and the distance of object can be calculated. However this technique also has difficulty in extracting information on the specular surfaces of internal organs.

To overcome the limitations associated with the above intra-operative imaging techniques, this paper proposes a novel optic-fiber based rolling indentation probe which is

capable of concurrently measuring the roller indentation depth and the tissue reaction force during the rolling.

B. The Design of the Rolling indentation probe

The rolling indentation probe consists of an optical fiber force sensor (FS), and four optical fiber displacement sensors (DS), DS-1, DS-2, DS-3 and DS-4. A spherical roller with a diameter of 6 mm is connected to the force sensor and can rotate freely. Fig.1 indicates the structure of the rolling indentation probe.

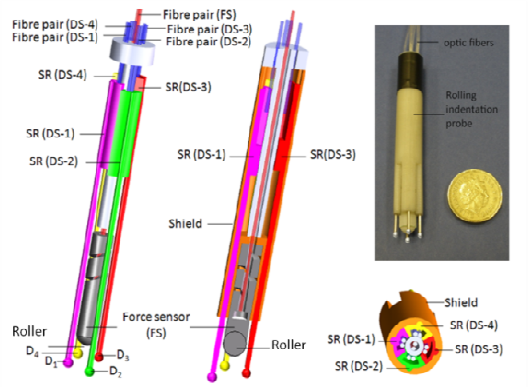

Fig.1. The rolling indentation probe consisting of one optical fiber force sensor (FS) as well as four optical fiber displacement sensors (DS), a coin of one pound sterling is used to indicate the size of the miniaturized Rolling indentation probe.

The sensing principles for both force and displacement measurements are based on the light intensity modulation scheme [38]. This scheme consists of a pair of transmitting fiber and receiving fiber as well as a reflector. The transmitting fiber carries the light generated from a light source and projects the light to the reflector. The reflector then reflects the light into the receiving fiber, and finally the intensity of reflected light is detected by an optical detector. Since the change of the displacement between the reflector and fiber tips varies the reflected light intensity, the motion of reflector can be detected through the measuring the reflected light intensity [39]. The transmitting and receiving fibers can be placed with an inclined angle φ to increase the sensitivity. It has been demonstrated in [38, 39] that, along the increase of the bent angle φ from 0^o to 90^o, the sensing sensitivity increases and displacement sensing range decreases.

The fiber optical FS is composed of a spherical roller, a helical-cut sensing structure attached with a reflector and a fiber pair including a transmitting fiber and a receiving fiber, as shown in Fig. 2(a). The helical-cut sensing structure behaviours like a spring with high axial stiffness (elastic modulus = 9.9 MPa); when an axial force is imparted, the helical-cut sensing structure is compressed, causing a small displacement of reflector towards the fiber tips. By measuring this displacement, the applied axial force can be interpreted. The tips of both transmitting fiber and the receiving fiber are bent with an angle of 15^o and placed towards each other to increase the sensitivity of the FS, Fig. 2 (a) (inclined angle $\varphi = 30^o$). The shield prevents the disturbance from lateral forces to the measurement of the axial force.

The four DSs, DS-1, DS-2, DS-3 and DS-4, are arranged in equal spaces inside the shield. SR(DS-1), SR(DS-2), SR(DS-3) and SR(DS-4) represent the sliding rods of DS-1, DS-2, DS-3 and DS-4, respectively. Four spheres, D_1, D_2, D_3 and D_4, connect with the sliding rods of the four DSs. The shield guides each sliding rod to move freely along its axial direction. Each DS consists of a sliding rod attached with a reflector and a pair of transmitting and receiving fibers for detecting the movement of the rods, Fig.2 (b). The two fibers are arranged in parallel with inclined angle $\varphi = 0^o$ to increase the displacement sensing range.

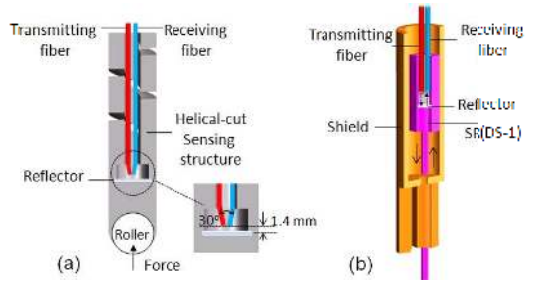

Fig.2. Schematics of the FS (a) and one of the DSs (b); in both sensors, a pair of transmitting fiber and receiving fiber is used to measure the distance between the fiber tip and the reflector. In the FS, the reflector is attached to a helical-cut sensing structure; in the DS, the reflector is attached to a sliding rod which has free movement axially.

Five high intensity LEDs are used for generating transmitting light, the change of light intensity for DSs and FS are measured using photo detectors, the received signals are amplified using the Op-Amp AD620. The optic circuit is placed inside metal box to reduce the signal noises. A 16-bit data acquisition card (NI PCI 6013) and the LabView^{TM} 8.0 software package are used to acquire the measured signals. The sampling rate is 100 Hz.

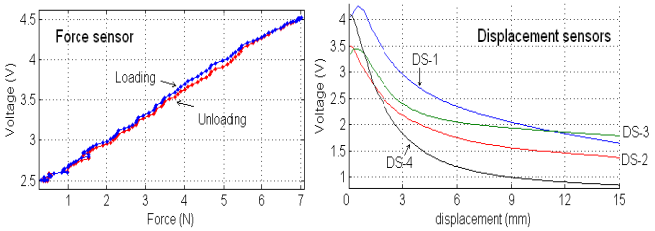

Fig.3. The calibration results of fiber optic FS (a) and four DSs (DS-1, DS-2, DS-3 and DS-4) (b) showing the measured voltages and corresponding changes in forces and displacements of the DSs.

To calibrate the four DSs and the FS of the rolling indentation probe, the entire unit is attached to the distal tip of the Mitsubishi RV-6SL manipulator, to allow for accurate motion control. For force sensing calibration, the FS is compressed against an ATI Mini40 sensor. During the calibration, the FS was slowly advanced towards and retrieved from the Mini40, varying the interaction force between the two sensors. The signals measured from the fiber optic FS and the corresponding force values measured from the Mini40 were recorded. The calibration results are shown in Fig. 3(a). For the calibration of the four DSs, each sliding rod of DS was moved increasingly from its minimum length to the maximum length over a range of 15 mm. the displacement h_1, h_2, h_3 and h_4 and the corresponding signal

from each sliding rod were recorded respectively. The calibration results are shown in Fig. 3(b).

C. Principle of Measuring the Indentation Depth and the Sensor Orientation

The probe is designed to non-invasively identify tumors buried in large solid organs such as liver and kidney employing small indentation depths. Thus in this study the soft tissue organ which the probe will roll over is assumed to have the following properties: surface curvature is much larger than the diameter of the probe ball; no hard edges or hard object in the investigated area on the surface; the tumor is embedded beneath the surface and no lump is showing on the tissue surface; the normal tissue of the organ is isotropic, homogenous and incompressible. Moreover the normal tissue is assumed to be linear elastic since biological tissues exhibit linear elasticity with small deformation [41].

When the probe indents into a soft tissue surface, the fiber optical FS measures the forces acting on the roller, the four spheres (D_1, D_2, D_3 and D_4) which are free to slide axially, are pushed to slide upward by the surrounding tissue. Due to soft tissue's high local deformability, the indentation contour raises from the indentation point to the tissue surface following an exponential curve [47], Fig.4. Therefore, by measuring the distance between the deepest indentation point of the roller and the positions of four spheres, the indentation depth of the roller and the orientation of the probe with respect to the tissue surface can be established.

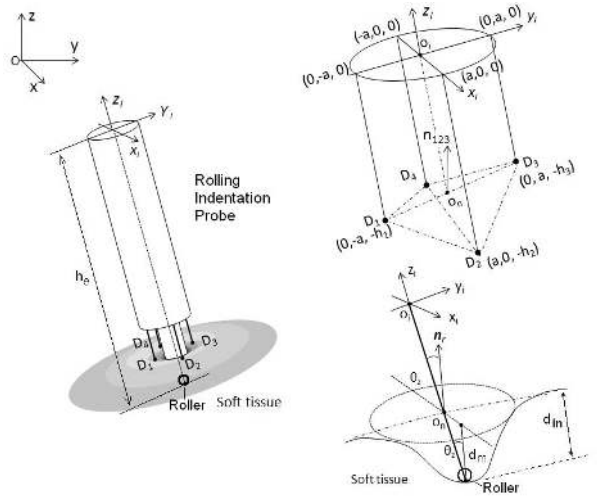

Fig .4. Measuring the indentation depth and the orientation of the probe with respect to the tissue surface; positions of spheres, D_1 D_2, D_3 and D_4 are (0, -*a*, -h_1), (*a*, 0, -h_2), (0, *a*, -h_3) and (-*a*, 0, -h_3) respectively in the coordinate system (x_i, y_i, z_i),where *a* is the outer radius of the probe (*a* = 5.5 mm), h_1, h_2, h_3 and h_4 are the distances between the spheres and the x_i y_i –plane; o_n indicates the average position of the four spheres.

It is defined the (*x, y, z*) to be the globe Cartesian coordinate system. The coordinate system (x_i, y_i, z_i) is attached to the rolling indentation probe as indicated in Fig.4 (z_i is align with the central axis of the sensor). When the roller indents into the soft tissue, the four spheres can configure four planes, $D_1D_2D_3$, $D_2D_3D_4$, $D_1D_2D_4$ and $D_1D_3D_4$. The normal direction of the contacted tissue surface can be approximated by averaging the normal vectors of the planes $D_1D_2D_3$, $D_2D_3D_4$, $D_1D_2D_4$ and $D_1D_3D_4$.

Defining the positions of spheres, D_1 D_2, D_3 and D_4 to be (0, -*a*, -h_1), (*a*, 0, -h_2), (0, *a*, -h_3) and (-*a*, 0, -h_3) respectively in the coordinate system (x_i, y_i, z_i),where *a* is the radius of the rolling indentation probe (*a* = 5.5 mm), h_1, h_2, h_3 and h_4 are the distances between the corresponding spheres and the x_i-y_i plane. As seen in Fig. 4, the four spheres construct four planes, $D_1D_2D_3$, $D_2D_1D_4$, $D_3D_4D_1$ and. Defining the $\boldsymbol{n}_{ijk}$ to be the unit vector normal to the plane $D_iD_jD_k$, where $(i,j,k) \in (1,2,3,4)$ and $i \neq j \neq k$, the $\boldsymbol{n}_{ijk}$ can be calculated as:

$$\boldsymbol{n}_{ijk} = \frac{D_jD_k \times D_iD_j}{\left|D_jD_k \times D_iD_j\right|}. \tag{1}$$

Defining $\bar{\boldsymbol{x}}$, $\bar{\boldsymbol{y}}$ and $\bar{\boldsymbol{z}}$ as the unit vectors along x_i axis, y_i axis and z_i axis, the unit vector normal for the four planes can be expressed as:

$$\boldsymbol{n}_{ijk} = \lambda\left[\frac{a(2h_j - h_i - h_k)}{r_{ijk}}\bar{\boldsymbol{x}} + \frac{a(h_k - h_i)}{r_{ijk}}\bar{\boldsymbol{y}}\right] + \frac{2a^2}{r_{ijk}}\bar{\boldsymbol{z}}, \tag{2}$$

where r_{ijk} is the norm of the vector $\boldsymbol{n}_{ijk}$,

$$r_{ijk} = \sqrt{a^2(2h_j - h_i - h_k)^2 + a^2(h_k - h_i)^2 + 4a^4}.$$

For plane $D_1D_2D_3$, i=1, j=2, k=3 and λ=1; for plane $D_2D_1D_4$, i=2, j=1, k=4 and λ= -1; for plane $D_3D_4D_1$, i=3, j=4, k=1 and λ=-1; for plane $D_4D_3D_2$, i=4, j=3, k=2 and λ= 1. The normal vector to the contacted tissue surface, $\boldsymbol{n}_r$, can be approximated by the resultant vector of $\boldsymbol{n}_{123}$, $\boldsymbol{n}_{214}$, $\boldsymbol{n}_{341}$, and $\boldsymbol{n}_{432}$. The angle θ_z between the normal vector of the tissue surface $\boldsymbol{n}_r$ and the z_i axis (central axis of the probe) can be determined as:

$$cos\theta_z = 2a^2\left(\frac{1}{r_{123}} + \frac{1}{r_{214}} + \frac{1}{r_{341}} + \frac{1}{r_{432}}\right), \tag{3}$$

Define a point o_n on the axis z_i and o_no_i equal to the average of the distances between the four contactors and the x_i-y_i plane, Fig. 4. The distance between the deepest indentation point of the roller to the normal plane of $\boldsymbol{n}_r$ where point o_n locates, d_m, is determined as:

$$d_m = co\ \theta_z\left(h_e - \frac{1}{4}\sum_{i=1}^{4} h_i\right), \tag{4}$$

where h_e is the distance between the tip of the roller and the x_i y_i -plane. Since the helical-cut sensing structure of the FS has high axial stiffness, the change of distance h_e during indentation is reasonable to be neglected. Hence distance h_e can be considered as a constant value. Moreover, the distance h_1, h_2, h_3 and h_4 can be measured using the corresponding DSs, DS-1, DS-2, DS-3 and DS-4. Thus the d_m and orientation of the probe with respect to soft tissue surface can be determined. To obtain the indentation depth, d_{in}, the relationship between the d_m and d_{in} need to be calibrated for different tissue samples. The calibration can be then used to interpret the indentation depth d_{in} from measuring the d_m. The calibration of d_m and d_{in} is described in detail in Section III.A.

D. Identify Stiffness using Tissue Reaction Force and Indentation Depth

The tissue stiffness can be represented using the tissue's elastic modulus and the linear elastic assumption of tissue allows the use of linear elastic contact theory to estimate the

tissue's elastic modulus through the measurements of tissue reaction force and indentation depth. Described in [45], using a rigid spherical indenter with small indentation, the elastic modulus of tissue can be estimated as:

$$E = \frac{3f(1+\nu)}{8d_{in}\sqrt{rd_{in}}}, \quad (5)$$

where E is the elastic modulus, f is the tissue reaction force normal to tissue surface, r is the radius of the sphere, d_{in} is the indentation depth and ν is the Poisson ratio. For incompressible material, ν =0.5.

To validate the linear elastic assumption, additional indentation tests were conducted on various soft tissues. The tested samples included pig liver, pig kidney, pig heart and silicone material made from the RTV6166 gel which has mechanical properties similar to those of biological soft tissue [40]. During tests, the spherical roller was indented into a test sample by 5 mm at the speed of 1mm/s, the motion of probe was controlled using the Mitsubishi manipulator. It was found that Eq.5 fits the measurement very well for the silicone sample (R-square error (R^2) =0.99); for biological tissues, Eq. 5 is accurate when the indentation depth is small (R^2 >0.97 when d_{in} < 3.5 mm), Fig.5. Using Eq.5 the elastic moduli of the heart, silicone, kidney and liver are estimated as 38.7 KPa, 29.5 KPa, 21.3 KPa and 8.5 KPa. The estimated elastic moduli of kidney and liver are in good agreement with existing literatures [18, 25, 46]. To further validate the linear elastic assumption of tissue, the indentation speed was varied from 0.1 mm/s to 20 mm/s. It was found that the estimated elastic modulus has no significant correlation with the indentation speed for all the tissue samples (|correlation| < 0.138, the correlation is a number from -1 to 1, ±1 indicates a perfect linear correlation, 0 indicates no correlation). Similar observations have been made elsewhere [10, 13]. Thus the elastic modulus estimation can be assumed to be independent of the indentation speed. The above validation tests demonstrate that when the indentation depth is small (<3.5 mm), the elastic contact theory is valid for estimating the tissue elastic modulus.

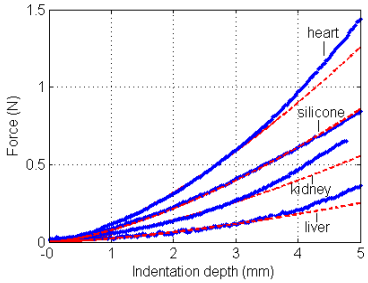

Fig.5. The relation of tissue reaction force and the indentation depth of the sphere; the solid lines are the experimental measurements, the dashed lines are the estimations using Eq.5.

III. Experiments of Indentation Depth Measurement

A. Calibrating the Relation of d_{in} and d_m

It is expected that the relation of the d_{in} and d_m can be varied for different soft tissues. Thus calibrating such relation is required prior operation. Moreover, as the probe is designed to scan a tissue with varying stiffness, thus the correlation between the tissue stiffness and the relation of d_{in} and d_m needs to be investigated. As such, tests were conducted on four silicone samples with different stiffness (Si-1, Si-2, Si-3 and Si-4). These silicones were made from the RTV6166 gels. The elastic moduli of Si-1, Si-2, Si-3 and Si-4 were measured as 8.75 KPa, 17.5 KPa, 29.5 KPa and 50.4 KPa respectively. All the silicone samples are cuboids with the dimension of 30 mm in height, 100 mm in width and 100 mm in length, Fig.6. For calibration, the probe was vertically indented into a silicone sample at a speed of 1 mm/s until d_{in} reached 5 mm. The d_{in} and the corresponding d_m were measured during the indentation and the above procedures were repeated three times for each silicone sample.

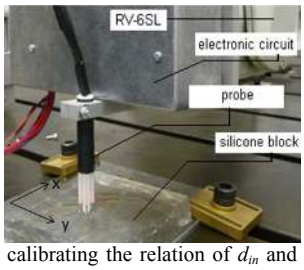

Fig.6. The setup for calibrating the relation of d_{in} and d_m using the rolling indentation probe, the robotic manipulator and silicone samples.

The relation of d_{in} and d_m was modeled using an exponential function described in [41]:

$$d_{in} = \alpha\left(e^{\beta d_m} - 1\right), \quad (6)$$

where α and β are the coefficients to need be calibrated for different tissues as they are related to the tissue mechanical properties, size of indenter and the placement of contactors. It was found that Eq.6 provides accurate approximation for all the samples (R^2 >0.99). Coefficient α was estimated as1.87 for Si-1, 1.72 for Si-2, 1.54 for Si-3 and 1.26 for Si-4; coefficient β can be fixed to 0.45 for all the samples.

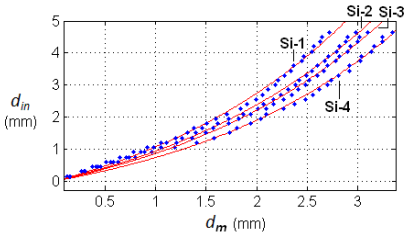

Fig.7. The relation of d_{in} and d_m; the blue dots are the averaged measurements from three tests and the solid red lines are the fitted curves.

As shown in Fig.7, at same indentation depth d_{in}, the measured d_m increases as the increase of tissue stiffness. This indicates that if the probe is calibrated on a low stiffness area, it will over-estimate the d_{in} for high stiffness regions. Fig.8 (a) shows that using the calibration result of Si-1(E = 8.75 KPa), the over-estimation of d_{in} increases along with the increase of tissue stiffness. Assuming the probe is rolling on a tissue area with elastic modulus of E and the indentation depth is d_{in}, the reaction force f is $8E\sqrt{r}d_{in}^{1.5}/3(1+\nu)$, Eq.5. Substituting f into Eq.5 and assuming the estimated indentation depth is d_{in}^e, the estimated elastic modulus E^e can be derived as:

$$E^e = E\left(\frac{d_{in}}{d_{in}^e}\right)^{\frac{3}{2}} \quad (7)$$

Eq.7 implies that the over-estimation of d_{in} for stiffer area could cause the elastic modulus of this region being

under-estimated. However, as shown in Fig.8 (b), the estimated elastic modulus has an incremental relationship with the ground truth of stiffness. This indicates that the probe is capable of differentiating soft tissue stiffness, while the estimation error of tissue elasticity increases along with the raise of tissue stiffness.

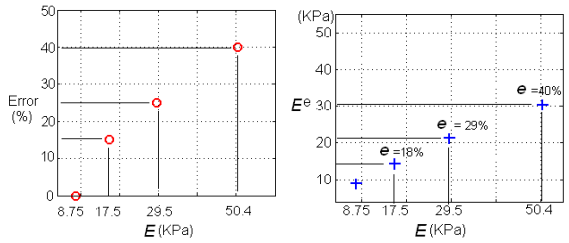

Fig.8. The estimation errors in indentation depth sensing (a) and in tissue elastic modulus identification (b) along with the increase of tissue stiffness; E is the real tissue elastic modulus , E^e is the estimated elastic modulus, e is the estimation error of elastic modulus.

B. Measurement of Indentation Depth

1) Accuracy with Different Rolling Orientation of Probe

In order to examine the accuracy of measuring the indentation depth using the rolling indentation probe, preliminary validation tests were conducted on the silicone sample Si-2.

Firstly, the tests were conducted to investigate the accuracy in measuring indentation depth with different probe orientation during rolling indentation. During tests, the robotic manipulator was used to drive the probe to slide across the silicone sample along y axis by a distance of 35 mm at different angle θ_z (the angle between the normal vector of the silicone surface and the axial direction of the probe). There were three angle selected, $\theta_z = 0^o$, 10^o and 20^o. In order to determine the exact point of touch, a surface registration was carried out prior to tests by setting multiple waypoints on the rolling path as described in previous work [25]. During the sliding, the indentation depth was linearly increased from 0 mm to 4 mm. At each angle θ_z, the experiment was repeated three times. Fig.9 shows the comparison between the measured indentation depth and ground truth data.

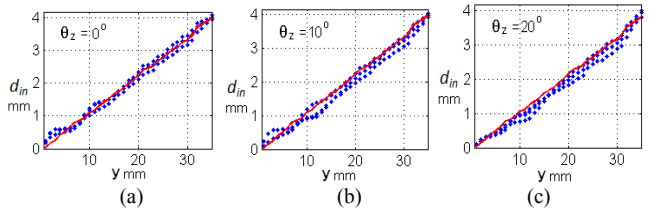

Fig.9. The comparison between the measured indentation depth (blue dots) and ground truth data (red solid line) with different angle θ_z including $\theta_z = 0^o$, 10^o and 20^o, showing in (a), (b) and (c) respectively.

For analyzing the measurement accuracy, the RMSE error is used. The RMSE error is calculated as:

$$RMSE = \sqrt{\frac{\sum_{j=1}^{n}(d_{in_j}^{e} - d_{in_j})^2}{n}}, \quad (8)$$

where n is the sample number.

The error analysis showed that the mean RMSE for $\theta_z = 0^o$ is 0.252 mm; the mean RMSE for $\theta_z = 10^o$ is 0.286 mm; the mean RMSE for $\theta_z = 20^o$ is 0.336 mm. It can be seen that, while the accuracy slightly decrease along with the increase of θ_z, the probe can measure the indentation depth reasonably well for each selected angle θ_z.

2) Accuracy with Different Approaching Angle of Probe

Furthermore, the accuracy in measuring indentation depth with different approaching angles was investigated. During tests, the orientation of the probe was adjusted by changing the angle of yaw θ_y and pitch θ_p, Fig. 10(a), and then the probe indented the silicone sample by 4.5 mm at a speed of 1 mm/s. The range of the θ_y and θ_p were chosen from 0^o to 20^o. Tests were conducted with different combinations of θ_y and θ_p. For each combination, tests were repeated three times. The results are summarized in Fig.10 (b). The results show that measurement accuracy decreases along with the increase of yaw and pitch angles (the RMSE increases from 0.21mm when θ_y and $\theta_p = 0^o$ to 0.4 mm when θ_y and $\theta_p = 20^o$). The experimental results indicate that the accuracy of indentation depth estimation is acceptable when the approaching angle varies within the range of (θ_y, $\theta_p \leq 20^o$).

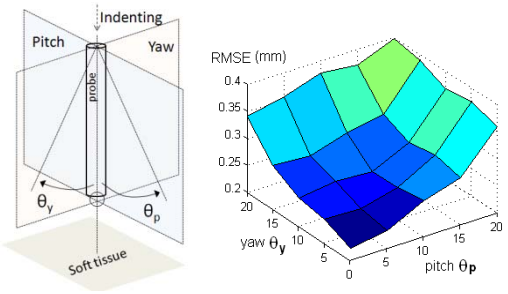

Fig.10. The change of approaching angle of probe by adjusting the yaw and pitch angle (a) and the RSME errors in measuring indentation depth with different approaching angles.

IV. Tissue Abnormality Identification from Rolling Indentation

The rolling indentation probe is developed for rapidly identifying tumors through rolling indentation without prior tissue surface registration. In this section, experiments were conducted to evaluate the performance of the probe for tumor identification. For this study, the normal tissue is modeled using silicone gels with elastic modulus varied from 8.5 KPa to 28 KP, similar to the stiffness of liver and kidney (see Section II.D). The simulated tumors are 1.8 to 8 times harder than the normal tissue. This is comparable to the tumor-tissue stiffness ratio for biological soft tissues [13].

A. Tumor Identification with varied Tumor Size and Depth

1) Experimental Protocol

First, the efficacy of tumor identification with respect to the size and depth of the embedded tumor was investigated. For this study, a silicone phantom with nine embedded spherical simulated tumors was constructed using the RTV6166 gel. The dimensions of the phantom and the size and embedded depth of tumors are shown in Fig.11. The elastic modulus of the tumor is 219 KPa. The silicone has a relative constant stiffness across the entire surface. By conducting multiple indentation tests on the tumor-free areas, the elastic modulus of the silicone was measured as 26.9 ± 4.6

KPa (the standard deviation = 1.78 KPa). The silicone phantom has an uneven surface and the average surface height along the z axis is 25 mm and the variation of the surface height = $\pm$ 1.04 mm).

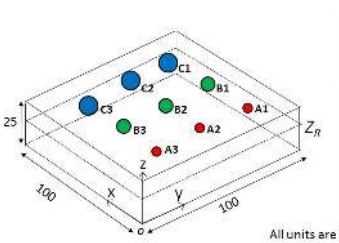

	Size (ϕ)	Depth
A1	3	2
A2	3	6
A3	3	10
B1	5	2
B2	5	6
B3	5	10
C1	8	2
C2	8	6
C3	8	10

All units are in 'mm', ϕ is diameter

Fig.11 Dimensions of the silicone phantom and the size and depths of the nine simulated tumors; Symbol "o" indicate the origin of the Cartesian coordinate system.

Previous results show that deep rolling indentation depth facilitates tumor identifications [25]. However for the linear elastic assumption of tissue to be valid, a small indentation depth is required. Moreover, it was found that the accuracy and repeatability of tumor identification were insensitive to changes in rolling speed in the range from 15 mm/s to 60 mm/s [25]. Therefore, the maximum indentation depth was set at 4 mm and the rolling speed of the probe was selected as 30 mm/s in this study.

Prior to tests, the roller of the probe was programmed to follow multiple paths defined on a plane which is parallel to the x-y plane shown in Fig.11. During experiments, the probe was kept perpendicular to this plane. The distance from this plane to the x-y plane is Z_R. Z_R was selected as 22 mm causing the indentation depths ranged from 2 mm to 4 mm. The average indentation depth was 3 mm. On this plane where the roller travelled, a series of 30 paths parallel to the y axis were defined, with a shift of 3mm along the x axis between each path. Each path is 90 mm in length to cover an area of 90×90 mm^2 and the initial path starts at position (x = 10 mm, y = 10 mm, Z_R = 22 mm). To evaluate the robustness and repeatability of the probe, rolling indentation experiments were repeated six times.

2) Tumor identification from Stiffness Map

After each test, the estimated tissue elastic moduli along the rolling path were fused together to generate a stiffness map of the examined tissue as described in [25]. As tumors are stiffer than the surrounding silicone, locations of tumors show up as high stiffness regions (red colour) on the map.

To highlight the advantage gained when employing the developed probe, the stiffness map is compared with the force map generated directly from the tissue reaction forces recorded along the rolling paths and assuming the rolling indentation depth was constant at all the times. Fig.12 shows the comparison between the stiffness map and the force map. It can be seen that a high force area (highlighted in dashed circle) appears in the force map despite the fact that the stiffness of the silicone is most uniform across the entire surface. The observed force changes across the phantom are due to variations in rolling indentation depths. In the stiffness map, this high force region caused by the increase of the rolling indentation depth is eliminated and stiffness of the silicone (except the regions with tumors) appears uniform, thus the increased stiffness caused by the presence of a tumor is more easily identifiable. The above comparison also indicates the developed probe can compute the tissue stiffness without requiring constant rolling indentation depth, hence without the need of prior tissue surface registration.

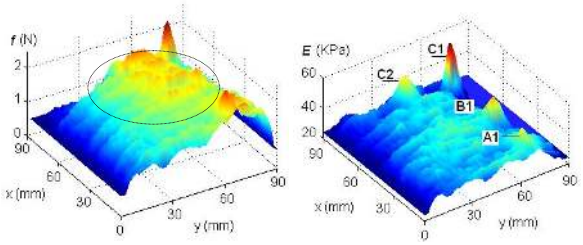

Fig.12 The comparison between the force reaction map (left) and the stiffness map produced by the rolling indentation probe (right) with the average rolling indentation depth of 3 mm.

To identify the locations of tumor from the stiffness map, an image threshold is applied. The image regions, in which pixel values exceeded the threshold, are considered areas that contain tumors. The location of a tumor is determined by calculating the centroid for each image region. The remaining areas were regarded as the nodule-free, Fig.13.

Assuming the elastic modulus of the normal tissue, i.e. the silicone, follows a normal distribution, 99.7% observation will fall within the range of $\bar{E} \pm 3s_E$ [48] ($\bar{E}$ is the mean of measured elastic modulus of the silicone, s_E is the standard deviation of elastic modulus measurements). Thus the image threshold T_r is determined as:

$$T_r = \bar{E} + 3s_E, \tag{9}$$

Clinically, $\bar{E}$ and s_E could be determined by measuring the elastic modulus of the healthy tissue multiple times prior to the rolling indentation.

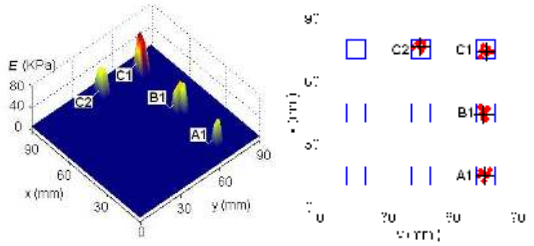

(a) (b)

Fig.13. Tumor identification employing the image threshold for one test (a) and the results of tumor identification from six repeated tests (b); In Fig.13 (b), dots are the identified locations of tumors for each experiment, crosshairs are the average locations of six experiments

As was mentioned above, test was repeated six times. To illustrate the repeatability of the technique, the locations of the identified tumors from the repeated tests are shown in Fig. 13 (b). Where no tumor can be identified, the location is left blank although the ground truth tumor location is marked with a square.

3) Summary

Comparing with the ground truth, the errors of the identified tumor locations are ranged from 0.16 mm to 2.32 mm in x axis and from 0.31 mm to 2.67 mm in y axis. The standard deviations of the identified tumor locations are ranged from 1.25 mm to 2.33 mm along the x axis and from 0.81 mm to 2.43 mm along the y axis. This indicates that the locations of the identifiable tumors on stiffness map are

consistent with the actual locations and results of tumor identification are repeatable. Furthermore, it was found that the probe is sensitive to the existence of a small tumor buried near the surface, as it can identify a tumor of 3 mm in diameter embedded 2mm below the surface. However, the results also show that probe is not effective in identify small and deep embedded tumors. This suggests that a sensitivity threshold of the probe does exist. This threshold is a function of the tumor size, the buried depth of the tumor, the rolling indentation depth and relative variation in tumor stiffness when compared with the normal tissue. More in-depth evaluation of these effects for real tissue organ tests is required to be carried out in future.

B. Tumor Identification with varied Stiffness Ratio between Tumor and Normal Tissue

To investigate the effects of the stiffness ratio between the tumor and the normal tissue to the tumor identification using the developed probe, five silicone phantoms (SP1, SP2, SP3, SP4 and SP5) with different tumor-tissue stiffness ratios were constructed. The silicone phantoms are cuboids with the same dimensions (height =30 mm, width = 40 mm, length = 60 mm). The tumors are spherical balls buried beneath the phantom surface with a depth of 2 mm. The elastic modulus of tumors is 50.4 KPa. Fig. 14 lists the information regarding the tumor-tissue stiffness ratios and size of the embedded tumors for each silicone phantom. Prior to tests, multiple rolling paths were defined on the each phantom surface. Twelve paths parallel to the x axis were defined, with a shift of 2mm along the y axis between each path. Each path is 45 mm in length, hence an area of 24×45 mm^2 is covered. During experiments, the probe was rolled over the phantom following the predefined paths and kept perpendicular to the surface. The rolling indentation depth was 3.5 mm and the rolling speed was 30 mm/s. The initial path starts at position (x = 8 mm, y = 8 mm). To evaluate the robustness and repeatability, the rolling indentation tests were repeated three times for each phantom.

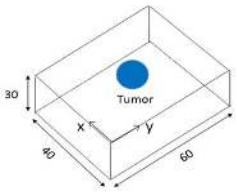

Phantom	E of silicone	Tumor-tissue Stiffness ratio	Diameter of tumor
SP1	8.5 KPa	5.9	8 mm
SP2	18.6 KPa	2.7	8 mm
SP3	27.9 KPa	1.8	8 mm
SP4	28.2 KPa	1.8	5 mm
SP5	28.1 KPa	1.8	3 mm

Fig.14 Dimensions of the silicone phantom and information regarding the tumor-tissue stiffness ratios and size of the embedded tumors for each silicone phantom.

After tests, tumor identifications through rolling indentation were conducted as described in Section IV.A. The results show that the tumors in SP1, SP2, SP3 and SP4 were successfully identified using the probe. This demonstrates that the probe is effective for identifying tumors even with small tumor-tissue stiffness ratio. As shown in Fig. 15, the probe is capable of detecting a tumor of 5 mm in diameter when tumor is only 1.8 times stiffer than normal tissue.

It was also found that the higher the tumor-tissue stiffness ratio is, the easier it is to identify the tumor from the stiffness map. For instance, the probe is capable of locating a tumor of 3 mm in diameter when the tumor-tissue stiffness ratio is 8 but unable to identify the same size tumor when the tumor is 1.8 time stiffer than the tissue. As shown in Fig. 15, the difference in estimated stiffness between the tumor region and tumor-free areas reduces along with a decrease of the tumor-tissue stiffness ratio.

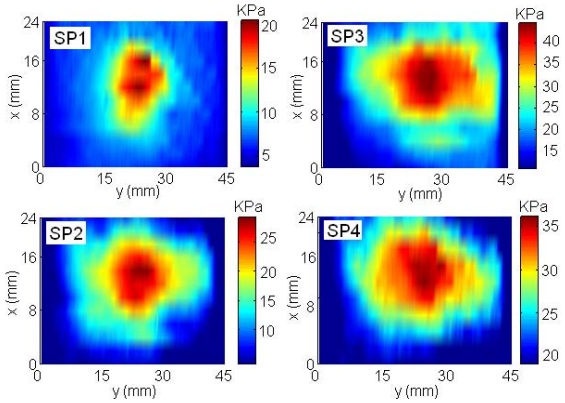

Fig.15. The stiffness map generated from different silicone phantoms; locations of tumors show up as high stiffness regions (red colour) on the map.

V. Conclusion and Discussion

This paper introduces a novel rolling indentation probe which can measure both the indentation depth and the tissue reaction force during rolling indentation. Test results show that this probe is accurate and has good repeatability in measuring rolling indentation depth. Tests also indicate that employing the rolling indentation probe for rolling indentation allows the stiffness distribution of the investigated soft tissue to be identified and visualized in form of a stiffness map, without prior registration of the tissue surface. Following our feasibility study on the silicone phantom, it can be concluded that tumor identification using the rolling indentation probe is effective and accurate. If applied in MIS, it has the potential to aid surgeons considerably in procedures that involve the accurate targeting of malignant areas [42] and identification of precise margins for curative resection [43], and in improving their intra-operative diagnostic and interventional decisions.

Several limitations need to be considered. First, there are a several assumptions made for the soft tissue organ which the probe will roll over. For larger tumors and those that actually form an edge on the organ tissue those assumptions may not hold and the estimated tissue stiffness may be erroneous. Still for such cases, larger tumors is likely to show up on the stiffness map. Second, the probe has difficulties to identify small tumors that are deeply buried inside the soft tissue. However, tumors, even small ones that are fairly close to the surface (about 2 mm deep) will be identifiable and thus our approach is complementary to vision-based systems. Further, cost-effectiveness is important in medical instrumentation and for a probe like ours with its rolling and moving parts, this may be difficult to achieve initially; however, with the introduction of more advanced design and fabrication methods (similar to those used in current medical tools) and when moving towards mass production the production will certainly become more cost effective. In addition, the aim of this paper was to show the advancement in rolling indentation

for MIS with its clear benefits for tumor detection and localization. When changing tools (i.e. from rolling indention probe to a scissor-type tool) some of the information acquired might be lost. This issue may be overcome in future by integrating a surgical tool with rolling indentation capabilities similar as proposed here.

To further improve the rolling indentation probe, future development will be conducted on several aspects. First, the contact between the contactor and the soft tissue is maintained by gravity for the prototype described in this paper. This approach provided satisfactory results for the experimental study reported on in this paper where the probe was kept fairly normal to the silicone block's surface and it was ensured that the probe was pointing downwards at all times. However, in a more realistic situation it may not always be possible to keep the probe in the required downwards-pointing orientation – hence, for a practical usage of the probe, a mechanism such as springs or pressurized air chambers could be used to generate the necessary force to ensure that the indentation spheres are in contact with the tissue at all times during rolling indentation.

Second, the tilt of the reflectors with respect to the probe's axial direction causes considerable error in measuring indentation depth. This can to be reduced by increasing the rigidity and accuracy of the sensor mechanical structure.

Moreover, our previous research found that even when changing the contact angle during rolling indentation over a wide range ($\pm 60^{o}$), the ratio of rolling tangential force F_t over normal force F_n is almost constant (<0.01), thus the normal force dominates the resultant force signal F_r [25]. This indicates that if implementing a 3-axis force sensor, even for an uneven surface it is possible to accurately measure F_n without measuring or changing the orientation of the probe; instead force F_n can be approximated using the resultant force F_r. Since the probe can also measure the rolling indentation depth for different orientations, the stiffness of the examined tissue can be estimated, even if the contact angles vary. For the current design of the rolling indentation probe, the force sensor can only measure the axial force; therefore the probe was kept perpendicular to the surface during tissue abnormality identification. In the future, research will be carried out aiming at developing a 3-axis force sensor which can be integrated with the rolling indentation probe [49].

REFERENCES

[1] Uranues, S., et al. "Early experience with telemanipulative abdominal and cardiac surgery with the ZeusTM Robotic System", Euro. Surg., Vol. 34, pp. 190-193,2002

[2] Guthart,G. S. and Salisbury, J. K.Jr. "The IntuitiveTM telesurgery system: Overview and application" Proc. IEEE Int. Conf. Robotics and Automation, pp. 618-621,2000.

[3] Tabaie, H. A., et al. "Endoscopic coronary artery bypass graft (ECABG) procedure with robotic assistance" ,The Heart Surgery Forum, Vol. 2, pp. 310-317, 1999.

[4] Murphy, D. A., et al. J. Thorac. Cardiovasc. Surg., Vol. 132, pp. 776-781, 2006.

[5] Deml, B., Ortmaier, T. and Seibold, U. Ottawa, Ontario : The touch, and feel in minimally invasive surgery, IEEE Int. workshop on haptic audio visual environment, and their applications. pp. 33-38. 2005.

[6] Miller, A.P., et al. Tactile imaging system for localizing lung nodules during video-assisted thoracoscopic surgery. Proc. IEEE Int. Conf. Robot. Autom. pp. 2996–3001. Rome, 2007.

[7] Carter, T., et al. Application of soft tissue modelling to image-guided surgery, Medical Engineering & Physics, Vol. 27, pp. 893-909, 2005.

[8] McCreery, G. L. et al., Feasibility of locating tumours in lung via kinaesthetic feedback, Int. J. Med. Robotics Comput. Assist. Surg., Vol. 4, pp. 58-68. March 2008.

[9] A.M. Zysk, F.T. Nguyen, A.L. Oldenburg, D.L. Marks, S.A. Boppart, "Optical coherence tomography: a review of clinical development from bench to bedside.". Journal of biomedical optics 12 (5): 051403.2007

[10] J. Ophir, et al. "Elastography: ultrasonic estimation and imaging of the elastic properties of tissues." Proc Instn Mech Engrs Part H 213 (1999): 203-233.

[11] L.S. Taylor, B.C. Porter, D.J. Rubens, and K.J. Parker. "Three-dimensional sonoelastography: principles and practices." Physics Med Biol 45, no. 6 (2000): 1477–1494.

[12] B. Shan, A. Pelegri, C. Maleke, and E. Konofagou. "A mechanical model to compute elastic modulus of tissues for harmonic motion imaging." Journal of Biomechanics 41, no. 10 (2008): 2150 – 2158.

[13] T. A. Krouskop, T. M. Wheeler, F. Kallel, B. S. Garra, and T. Hall, "Elastic moduli of breast and prostate tissues under compression," Ultrason. Imag., vol. 20, no. 4, pp. 260–274, 1998.

[14] E. B. Mendelson, J. Chen, P. Karstaedt. Assessing tissue stiffness may boost breast imaging specificity. Diagnostic Imaging. 2009;31(12):15-17

[15] A. M. Sabatini, P. Dario, and M. Bergamasco, "Interpretation of mechanical properties of soft tissues from tactile measurements," in Experimental Robotics. vol. 139, 1990, 152-162.

[16] J. Dargahi, S. Najarian, V. Mirjalili, and B. Liu, Modeling and testing of a sensor capable of determining the stiffness of biological tissues, Canadian Journal of Electrical and Computer Engineering, Canada Vol. 32, No. 1, 2007, pp. 45-51, Canada.

[17] K. Xu and N. Simaan. An Investigation of the Intrinsic Force Sensing Capabilities of Continuum Robots. In IEEE Transaction on Robotics, Vol. 24, No. 3, pp:576-587, 2008.

[18] B Hannaford, J Trujillo, M Sinanan, et al. "Computerized endoscopic surgical grasper". In Medicine Meets Virtual Reality, Westwood JD, Hoffman HM, Stredney D, et al. (eds). IOS Press: Amsterdam, The Netherlands, 265–271,1998.

[19] A Bicchi, G Canepa, D De Rossi, et al., "A sensor-based minimally invasive surgery tool for detecting tissue elastic properties", In IEEE Int. Conf. Robot. Autom., Minneapolis, MN, USA; pp.884–888. 1996;

[20] V. Egorov, S. Ayrapetyan, and A. P. Sarvazyan, "Prostate mechanical imaging: 3-D image composition and feature calculations," IEEE Transactions on Medical Imaging, vol. 25, pp. 1329-1340, 2006.

[21] V. Egorov and A. P. Sarvazyan, "Mechanical Imaging of the Breast," IEEE Transactions on Medical Imaging, vol. 27, pp. 1275-1287, 2008.

[22] P. S. Wellman and R. D. Howe, "Extracting Features from Tactile Maps," Proceedings of the Second International Conference on Medical Image Computing and Computer-Assisted Intervention, vol. Volume 1679/1999, pp. 11-33-1142, 1999.

[23] S. M. Hosseini, S. M. Towliat Kashani, S. Najarian, F. Panahi, S. M. Mousavi Naeini, A.Mojra, A medical tactile sensing instrument for detecting embedded objects with specific application for breast examination, Int. J. Med. Robotics Comput. Assist. Surg., Vol. 6, pp. 73-82, 2010

[24] R.A. Beasley, RD Howe. "Tactile tracking of arteries in robotic surgery". In Proc. IEEE Int. Conf. Robot. Autom., Washington, DC, vol.4: 3801–3806, 2002.

[25] H. Liu, D. Noonan, L. Seneviratne, P. Dasgupta, K. Althoefer, Rolling Indentation for Tissue Abnormality Localization during Minimally Invasive Surgery, IEEE Trans. on Biomedical Eng., **57**(2). 2010 pp. 404 - 414.

[26] Liu, H., et al. "The Rolling Approach for Soft Tissue modeling and Mechanical Imaging during robot-assisted Minimally Invasive Surgery" ,Proc. IEEE Int. Conf. Robot. Autom. ,pp. 846-850, 2008.

[27] Noonan, D. and H. Liu, Y. Zweiri, K. Althoefer, L. D. Seneviratne. A dual-function wheeled probe for tissue viscoelastic property identification during minimally invasive surgery, Proc IEEE Int. Conf. Robot. Autom. pp. 2629-2634, 2007.

[28] Sangpradit, K. Liu, H. Seneviratne, L. Althoefer, K., "Tissue Identification using Inverse Finite Element Analysis of Rolling Indentation" IEEE Int. Conf. on Robotics and Automation, (ICRA), Kobe, Japan, 2009

[29] Pohlenz, P, et al. “Major mandibular surgical procedures as an indication for intraoperative imaging”, J Oral Maxillofac Surg, Vol. 66, pp. 324-329, 2008
[30] Love, G. J., Pillai, A. and Gibson, S. “Use of the mini C-arm for wrist fractures--establishing a diagnostic reference level”, Radiat Prot Dosimetry, Vol. 128, pp. 309-311,2008
[31] Moore, A. J. and Newell, D. W. “Neurosurgery: principles and practice” , Springer, pp. 123-138,2005.
[32] Jain, A, et al. “ Intra-operative 3D guidance in prostate brachytherapy using a non-isocentric C-arm”, Int Conf Med Image Comput Comput Assist Interv., Vol. 10(Pt 2), pp. 9-17,2007.
[33] Keller, K. and Ackerman, J. “Real-time Structured Light Depth Extraction”, SPIE proceedings. pp. 11-18, 2000.
[34] Mourgues, F., Devernay, F. and Coste- Manière, E. “3D reconstruction of the operating field for image overlay in 3D-endoscopic surgery” ,Proceedings of International Symposium on Augmented Reality. pp. 191-192, 2001.
[35] Stoyanov, D, Darzi, A and Yang, G.Z. “A practical approach towards accurate dense 3D depth recovery for robotic laparoscopic surgery”, Comput Aided Surg, Vol. 10, pp. 199-208, 2005.
[36] Hu, G. and Stockman, G. 4 “3-D surface solution using structured light and constraintpropagation”, IEEE Transactions on Pattern Analysis and Machine Intelligence, Vol. 11, pp. 390-402, 1989.
[37] Lavoie, P., Ionescu, D. and Petriu, E.M. “3D object model recovery from 2D images using structured light”, IEEE Transactions on Instrumentation and Measurement, Vol. 53, pp. 437- 443
[38] Puangmali, P., et al., Optical fiber sensor for soft tissue investigation during minimally invasive surgery. 2008. Proc. IEEE Int. Conf. Robot. Autom. pp. 2934-2939.
[39] Buchade, P.B. and Shaligram, A.D. Simulation and experimental studies of inclined two fiber displacement sensor. 2006, Sensors and Actuators A , Vol. 128, pp. 312–316.
[40] A. M. Okamura, C. Simone, and M. D. O’Leary, “Force Modelling for Needle Insertion into Soft Tissue,” *IEEE Transactions on Biomedical Engineering*, vol.51, no.10, pp: 1707-1716, 2004.
[41] Y. C. Fung. “Biomechanics: Mechanical Properties of Living Tissues”. New York: Springer-Verlag, pp.269-281, 1993.
[42] Scott H. J., and Darzi, A. Tactile feedback in laparoscopic colonic surgery. Br. J. Surg., 1997, 84, pp. 1005.
[43] Dunn, D. C. Digitally assisted laparoscopic surgery. Br. J. Surg., 1994, 81, pp. 474.
[44] H. Liu, J. Li, Q. Poon, K. Althoefer, L. Seneviratne, “Miniaturized Force-Indentation Depth Sensor for Tissue abnormality identification” presented at IEEE Int. Conf. on Robotics and Automation 2010.
[45] A. Gefen, S.S. Margulies, Are in vivo and in situ brain tissues mechanically similar?, Journal of Biomechanics 37 (2004) 1339– 1352.
[46] Samur, E., Sedef, M., Basdogan, C., Avtan, L., Duzgun, O., A robotic indenter for minimally invasive measurement and characterization of soft tissue response, Medical Image Analysis vol.11 pp.361–373,2007.
[47] Johnson, K. L. Contact Mechanics. London: Cambridge, 1985.
[48] Miller, I., Probability and statistics for engineers 6th edition, Prentice-Hall 2000.
[49] Puangmali, P; A1thoefer, K; Seneviratne, L.D., Mathematical Modeling of Intensity-Modulated Bent-Tip Optical Fiber Displacement Sensors, IEEE Transactions on Instrumentation and Measurement, 59(2):283-291, 2010.

Hongbin Liu received the B.S. (Eng.) degree from the Northwestern Polytechnique University, Xi’an, China, in 2005, the MSc and Ph.D degree in 2006 and 2010 from Kings College London (KCL), UK.

He is currently a research associate in the Centre for Robotics Research, KCL. His research interests include intelligent grasping of robotic hand, interaction dynamics between surgical tools and soft tissue and the application of mechatronic system in medicine.

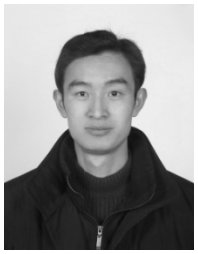

Jichun Li received the B.Eng. and the M.Eng degree from Chinese University of Geosciences(Wuhan), Hubei,China, in 2000 and in 2003 respectively. He is currently a Ph.D. student in the Centre for Robotics Research, Kings College London, UK. His research interests include interaction dynamics between surgical tools and soft tissue, sensor design for biomedical application and the design of mechatronic system in robotics.

Xiaojing Song obtained her PhD degree in mechanical engineering from King’s College London in 2010 and she is now a post-doc research associate at Centre for Robotics Research of King’s College London. Her research interests include dynamic modelling of mechatronics systems, robotic hand grasping and manipulation, robotics in surgical application.

Lakmal D. Seneviratne (M’03) obtained his B.Sc. (Eng.) and Ph.D. degree in mechanical engineering from King’s College London (KCL) where he currently is a professor in mechatronics at KCL.

His research interests include robotics and intelligent autonomous systems. He has published over 175 refereed research papers related to mechatronics. He is a Fellow of both the IET and the IMechE**.**

Kaspar Althoefer (M’02) holds a degree in electronic engineering from the University of Technology Aachen, Germany. He received his Ph.D. degree from the Department of Electrical and Electronic Engineering at King's College London (KCL) in 1997. He is now a Reader in the Department of Mechanical Engineering at KCL.

He has expertise in the areas of sensing, sensor signal analysis, embedded intelligence and sensor data interpretation using neural networks and fuzzy logic as well as robot-based applications. He has co-authored over 120 peer-reviewed research papers related to mechatronics.